Inhibition of AlF$_3$·3H$_2$O Impurity Formation in Ti$_3$C$_2$T$_x$ MXene Synthesis under a Unique CoF$_x$/HCl Etching Environment

Cody B. Cockreham,[†,‡,§] Xianghui Zhang,[†,‡] Houqian Li,[‡] Ellis Hammond-Pereira,[‡] Junming Sun,[‡] Steven R. Saunders,[‡] Yong Wang,[‡,∥] Hongwu Xu,[§] and Di Wu*[,†,‡,⊥,#]

†Alexandra Navrotsky Institute for Experimental Thermodynamics, Washington State University, Pullman, Washington 99163, United States

‡The Gene and Linda Voiland School of Chemical Engineering and Bioengineering, Washington State University, Pullman, Washington 99163, United States

§Earth and Environmental Sciences Division, Los Alamos National Laboratory, Los Alamos, New Mexico 87545, United States

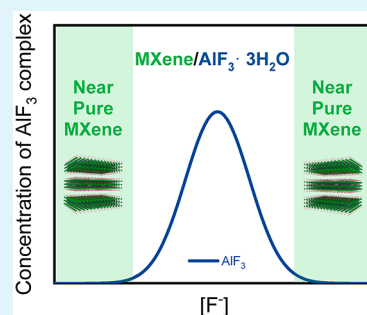∥Institute for Integrated Catalysis, Pacific Northwest National Laboratory, Richland, Washington 99352, United States

⊥Department of Chemistry, Washington State University, Pullman, Washington 99163, United States

#Materials Science and Engineering, Washington State University, Pullman, Washington 99163, United States
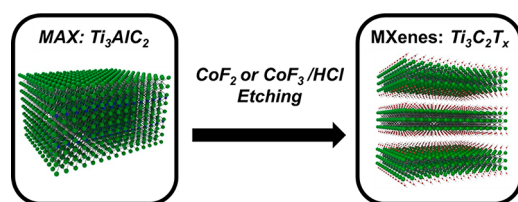
S *Supporting Information*

ABSTRACT: MXenes, most commonly transition metal carbides, are a family of two-dimensional (2D) materials with promising potential in, among other applications, supercapacitors and batteries. MXenes are synthesized by etching of aluminum or gallium layers in its parent MAX phase directly by HF or by HF *in situ* formation using a fluoride salt and strong acid. A commonly undesired byproduct of MXene synthesis is AlF$_3$·3H$_2$O. To relieve MXenes from AlF$_3$·3H$_2$O impurity, it is important to elucidate the factors that drive its formation. Here, we dually deduce the conditions that lead to AlF$_3$·3H$_2$O formation while exploring etching with cobalt fluorides (CoF$_2$/CoF$_3$). Previously uncharacterized, etching with cobalt fluorides offers a forthright method to etch MXenes while intercalating cobalt cations. The influence of this etching environment and AlF$_3$·3H$_2$O formation on MXene's structure, morphology, and surface bonding is investigated. Ionic strength of solution used for etching is found to be a critical driving factor in the formation of AlF$_3$·3H$_2$O impurity formation. Specifically, when the ionic strength falls between ∼8.5 and 10 M, AlF$_3$ complexation is stable. As a result, Ti$_3$C$_2$T$_x$ MXene phase with AlF$_3$·3H$_2$O impurity is obtained. In contrast, near-pure MXene is the only solid state product when *I* is smaller than 8.5 M or larger than 10 M. Hence, high purity MXene phase can be synthesized by subtle compositional tuning to manipulate the ionic strength of the etching environment.

KEYWORDS: *Ti$_3$C$_2$ MXenes, fluoride salt etching, layered materials, 2D materials, MAX phase, aluminum fluoride, cobalt fluoride, nanomaterials*

■ INTRODUCTION

A new two-dimensional layered early transition metal carbide was discovered in 2011 when Naguib et al. etched Ti$_3$AlC$_2$ with hydrofluoric acid (HF) to remove the aluminum at room temperature (RT), which chemically bound the titanium carbide layers together (see Figure 1).[1] This opened the door to a new group of layered materials dubbed MXene. MXene, of the form M$_{n+1}$X$_n$T$_x$, where M is an early transition metal such as Ti, V, or Mo; X is C or N; and T$_x$ is a capping end-group mostly −F, −OH, or ═O, is synthesized by the selective etching of a parent MAX phase, where A is most commonly aluminum.[2] When the aluminum is removed via etching, the remaining titanium carbide layers form an open 2D layered nanostructure with large interlayer space.[2] Owing to such 2D structure with accessible interlayer space, MXenes have promising potential applications, such as in lithium/sodium-ion batteries and supercapacitors and catalysis.[3,4] Therefore, the materials chemistry of etching is critical to tuning interlayer spacing and surface properties of MXenes.

Figure 1. Etching MAX using CoF$_2$ or CoF$_3$/HCl solution to synthesize MXene phases.

The most common methods of etching $Ti_3C_2T_x$ from Ti_3AlC_2 are directly with HF and by creating HF *in situ*, using an HF containing compound (i.e., NH_4HF_2) or a fluoride salt and a strong acid such as LiF/HCl, but can also be done with molten salts and strong bases.[2,3,5] Fluoride salt etching methods replace hazardous concentrated HF. Fluoride salt etching environments can modify the surface, morphology, and chemical reactivity of MXene.[2,6] In 2017, Wang et al. investigated a novel etching environment of MXene using FeF_3/HCl and also mentioned successful etching with CoF_2/HCl but did not elaborate.[7] It was found that iron(III) ions intercalated the MXene interlayer space and increased the water reactivity of $Ti_3C_2T_x$ toward the formation of TiO_2 anatase nanoparticles. Intercalating cobalt ions *in situ* intends to be advantageous, as the large cations could provide a stable expanded interlayer space as well as provide a building block for further processing of the MXene into a heterogeneous structure, for example, with oxidation of the cobalt ions into cobalt oxide particles. This approach provides a synthesis strategy for further nanochemical fabrication of MXenes. Interestingly, when etching with FeF_3, a significant amount of crystalline $AlF_3\cdot3H_2O$ phase after synthesis was observed and persisted through multiple washings with 6 M HCl.[7] It could be easily removed when washed for more than 1 h in deaerated water postfiltration. Crystalline $AlF_3\cdot3H_2O$ is a common undesired byproduct when etching aluminum-containing MAX phases. Postsynthesis treatments have to be taken to wash the MXene or extract the most pure and delaminated MXene particles by centrifugation.[7−9]

The conditions that lead to the formation of $AlF_3\cdot3H_2O$ have not been precisely identified with respect to its formation as a byproduct in the synthesis of MXene. Due to this knowledge gap, when formed, $AlF_3\cdot3H_2O$ currently requires postsynthesis treatment for removal. However, in 2008, Corbillon et al. demonstrated that Al^{3+} ions form complexes in water with F^- ions including AlF^{2+}, AlF_2^+, AlF_3, AlF_4^-, AlF_5^{2-}, and AlF_6^{3-}, of which AlF_3 is the only observed solid phase forming $AlF_3\cdot3H_2O$ in a hydrating environment.[10] The thermodynamic equilibria of complexation phases are strongly influenced by the ionic strength of the solution, and the speciation is correlated directly with the F^- content.[10,11] Crystalline $AlF_3\cdot3H_2O$ will form when the AlF_3 complex is thermodynamically favorable. By exploring the effect of temperature, time, and total weight percentage of MAX precursor using the traditional HF etching method, Rajavel et al. brushed insight into $AlF_3\cdot3H_2O$ formation conditions.[8] However, further experimental investigations into the detailed $AlF_3\cdot3H_2O$ formation mechanisms were not performed, which are essential and crucial toward successful industrial scale fabrication of MXenes. Therefore, understanding the factors that lead to the occurrence of a solid $AlF_3\cdot3H_2O$ byproduct in the synthesis of MXene is important to further the synthesis and processing of MXenes etched in fluoride environments.

Simultaneously, we explore the etching conditions that lead to $AlF_3\cdot3H_2O$ byproduct formation and present a preliminary characterization of cobalt fluoride etched MXenes. Variations in the ionic strength of solution during synthesis influence Al−F complexation greatly and influence the formation of $AlF_3\cdot3H_2O$. We used a suite of techniques to reveal the MXene etching conditions that led to $AlF_3\cdot3H_2O$ byproduct formation through stable AlF_3 complexation. The results have allowed the determination of the effects of cobalt fluoride etchants, high fluoride concentration, and ionic strength on the structure,

morphology, composition, and surface bonding of $Ti_3C_2T_x$ MXene and $AlF_3\cdot3H_2O$ byproducts. In light of these results, this study provides materials chemistry guidance for control of byproduct formation and use of transition metal fluorides as etchant sources in MXene synthesis.

■ MATERIALS AND EXPERIMENTAL METHODS

Materials Synthesis. Ti_3AlC_2 with a total weight percentage of 2, 4, or 6 was added to 20 mL of 6 M HCl and mixed in a 50 mL polypropylene test tube. CoF_2/CoF_3 with varying molar ratios was added gradually to the solutions in HF resistant test tubes to prevent overheating and reduce risk of HF exposure. When mixed, CoF_2/CoF_3 and HCl form HF in solution. Each solution was mixed for 30 s using a test tube agitator and then put into the bath sonicator for 30 min, after which the mixtures were heated to 60 °C for 48 h in a hood. The suspension was washed carefully with copious amounts of deionized water over a HF resistant vacuum filtration system and left to dry overnight. The samples were collected and dried in the vacuum oven at ∼60 °C. The samples are designated r-CoF_x/MAX-w where r is the molar ratio of cobalt fluoride salt to MAX phase, x is the stoichiometry of fluoride ions in the cobalt fluoride salt, and w is the total weight percent of original MAX phase. For example, using CoF_2 to etch a 4 wt % of MAX phase at a ratio of 2.3 CoF_2/MAX is designated 2.3-CoF_2/MAX-4.

Materials Characterization. The sample phases were identified by X-ray diffraction (XRD). Powder XRD data were obtained using a Rigaku Smartlab with Cu Kα radiation (k = 1.5406 Å) operated at a scan rate of 4°/min in the 2θ range of 5−80°. *In situ* XRD data were obtained using an Anton Paar XRK 900 furnace operated at a scan rate of 4°/min in the 2θ range of 5−65° with a heating rate of 10 °C/min under 50 mL/min of helium with hold times of 5 min and 1 h. Diffuse reflectance infrared Fourier transform spectroscopy (DRIFTS) spectra were obtained at 4 cm^{-1} resolution between 4000 and 600 cm^{-1} using Bruker Tensor 27 FTIR spectrometer. Scan time is 128 scans for all spectra. KBr was used to get the background at each temperature. About 20 mg sample (mixture of KBr and the solid products (SP) at weight ratio of KBr:SP = 10:1) was used. The sample was ramped to 50 °C at 10 °C/min with a hold time of 5 min under a helium flow of 50 cm^3/min. Thermogravimetry−differential scanning calorimetry−mass spectrometry (TG−DSC−MS) analyses were performed simultaneously via a Netzsch STA 449 F5 Jupiter coupled with a Netzsch QMS 403 D Aëolos. The measurements were carried out with a heating rate of 10 °C/min up to 600 °C under a nitrogen flow rate of 50 mL/min. The sample morphology was analyzed using scanning electron microscopy (SEM) using a Tescan Vega3 operated at 20 kV and 72 μA. The CoF_2 etched MAX was also analyzed by transmission electron microscopy (TEM), in which the MXene particles were dispersed in ethanol (3 mg MXene/mL ethanol). A 3 μL sample was taken and deposited on a 200 mesh formvar/carbon TEM grid. The grid was allowed to dry overnight at 40 °C under vacuum (300 mbar). A transmission electron microscope (FEI Tecnai T20) using a LaB$_6$ cathode was operated at 200 kV for imaging. Micrograph analysis was conducted using ImageJ (NIH).
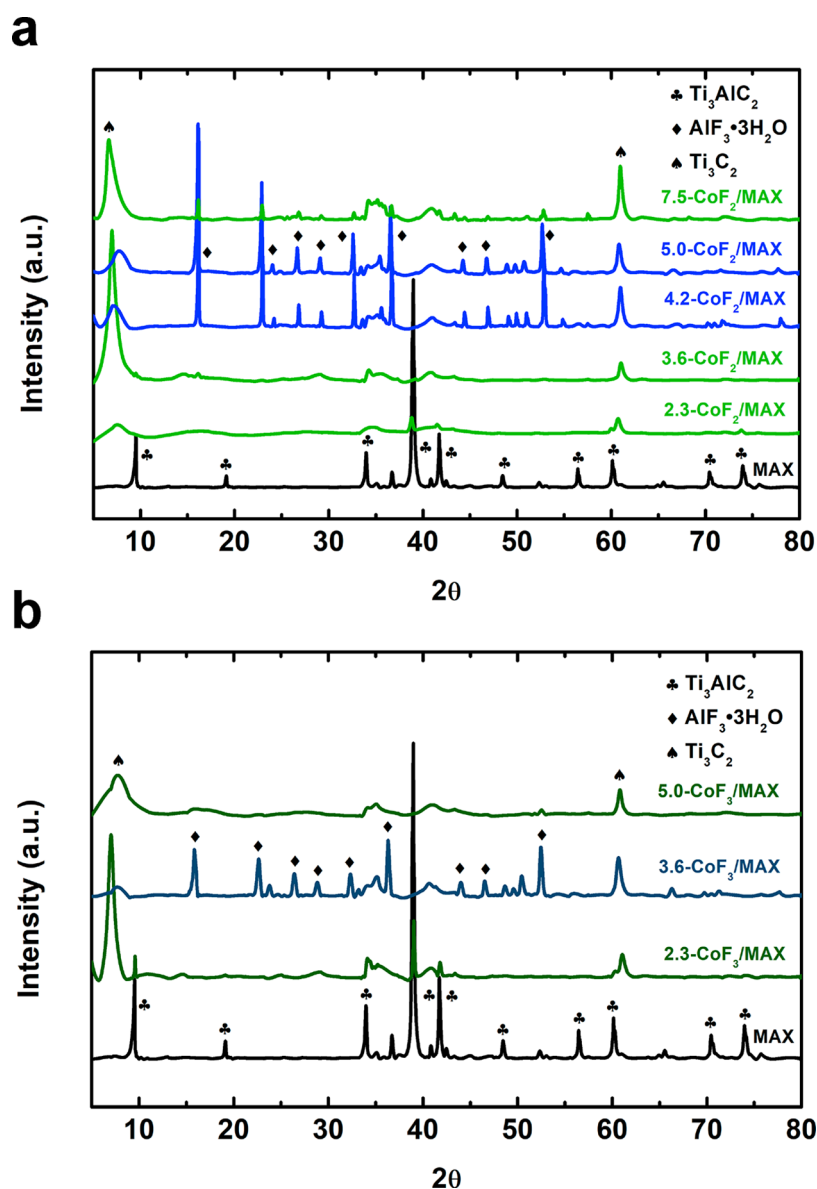
Ionic Strength Calculation. Ionic strength was determined by using eq 1:

$$I = \frac{1}{2} \sum_{i=1}^{n} c_i z_i^2 \tag{1}$$

where I is molar ionic strength, c_i is the molar concentration of ion i, and z_i is the charge number of that ion. For example, with a 20 mL of 6 M HCl solution and CoF_2/MAX ratio of 3.6, 1.75 g of CoF_2 is used. This corresponds to 0.775 M Co^{2+} and 1.55 M F^- in solution. By use of eq 1, the concentrations, and species charges, we find that the ionic strength of 3.6 CoF_2/MAX synthesis environment is 8.33 M.

■ RESULTS AND DISCUSSION

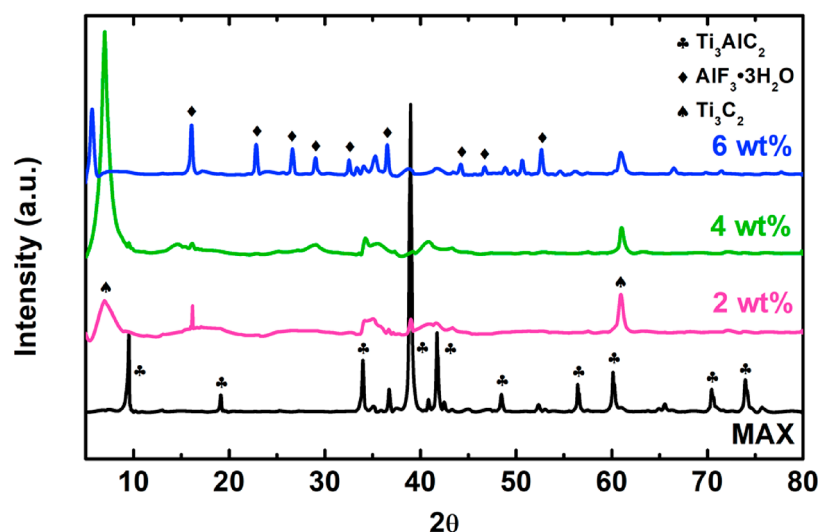First, powder XRD analysis was performed to identify the sample phase and structural evolution. Ti_3AlC_2 was etched

Figure 2. XRD patterns of MAX and MAX phases etched at a 4 wt % with different (a) CoF_2/MAX and (b) CoF_3/MAX molar ratios.

using CoF_2/HCl at 60 °C, creating HF *in situ*, which was similar to the synthesis described by Wang et al. (2017).[7] The CoF_2 to MAX ratio was modified while keeping the MAX constant at a 4 wt %. Similar approaches were used in other studies.[8,9] Figure 2a presents the XRD patterns of an array of CoF_2 etched samples. At a low CoF_2/MAX ratio (2.3), etching appears to be incomplete with MAX phase remaining. This is evidenced by the retention of the representative Ti_3AlC_2 peak at 39° and the low intensity of the $Ti_3C_2T_x$ peaks at 7° and 61°. Increasing the CoF_2/MAX ratio to 3.6 yields a well etched $Ti_3C_2T_x$ suggested by the sharp peak at 7° and the loss of Ti_3AlC_2 peaks. Further increasing the CoF_2/MAX ratio to 4.2 and 5.0 results in the formation of crystalline AlF_3·$3H_2O$ byproducts and a degradation of $Ti_3C_2T_x$ crystallinity (see Figure 2a). The $Ti_3C_2T_x$ peak at 7° corresponds to its (002) plane, whose *d*-spacing is one-half the *c* lattice parameter in its hexagonal closed packed geometry, thereby directly reflecting the interlayer spacing. The loss of intensity and the widening of this 7° peak imply a wider distribution of interlayer spacings in the AlF_3·$3H_2O$ rich samples. Further increase in the CoF_2/

MAX ratio to 7.5 leads to a relative lower amount of AlF_3·$3H_2O$ and $Ti_3C_2T_x$ with well-defined crystallinity. At moderate ratios, 4.2−5.0, the most AlF_3·$3H_2O$ byproduct was formed.

Upon replacing CoF_2 with CoF_3, the effect of etching on Ti_3AlC_2 was investigated. CoF_3 is strongly reactive with water. Co^{3+} is reduced into Co^{2+} which frees F^- ions to form HF with water. Effectively, etching with CoF_3 creates an environment of CoF_2/HCl and HF. $Ti_3C_2T_x$ etched by CoF_3 is shown in Figure 2b. Mirroring the CoF_2 etched Ti_3AlC_2, the low CoF_3/MAX ratio of 2.3 results in incomplete etching of Ti_3AlC_2 but does show high crystallinity of $Ti_3C_2T_x$ by its intense 7° peak. At a CoF_3/MAX ratio of 3.6, the AlF_3·$3H_2O$ phase appears. Further CoF_3/MAX ratio increase to 5.0 witnesses no strong AlF_3·$3H_2O$ peaks but does show an intense and broad 7° peak indicating a degradation in the layering of $Ti_3C_2T_x$. As the ratio of cobalt fluorides (CoF_2/CoF_3) increases, there exists a region in which the evolving ionic strength and fluoride ion concentrations enable a region of stable equilibrium for the speciation and subsequent crystallization of AlF_3 into AlF_3·$3H_2O$. At low concentrations (ratios of 0.5 and 1.0), a lack of
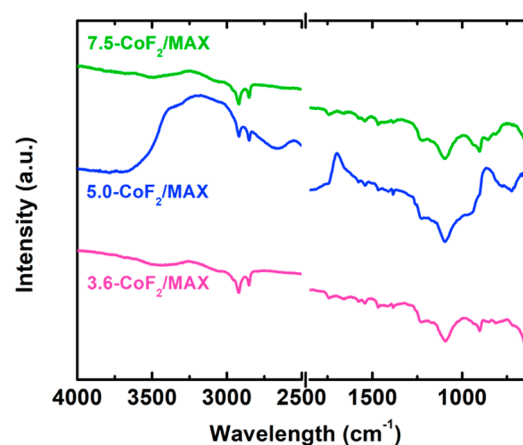
Figure 3. XRD patterns of MAX phases etched at a 3.6 CoF_2/MAX ratio at different total MAX weight percentages. The XRD patterns of MAX phase are also included for comparison.

fluoride ions in solution, reducing HF formation, prevents complete etching of the MAX phase (see Figure S1). Mirroring the trend seen when etched with CoF_2, the high and low etching ratios show very limited or no discernible $AlF_3 \cdot 3H_2O$.

The dependence of product phases on the concentration of Ti_3AlC_2 (MAX) was investigated by maintaining a 3.6 CoF_2/MAX ratio and varying the amount of MAX (see Figure 3). At the low 2 wt %, the MAX presents poor etching, probably due to a lack of fluoride ion concentration from the lower corresponding CoF_2 in solution. As the weight percentage increases, near-pure $Ti_3C_2T_x$ is formed at 4 wt %. Increasing to 6 wt % results in high amounts of $AlF_3 \cdot 3H_2O$. No discernible trend was found linking $Ti_3C_2T_x$ lattice parameters or unit cell volume with synthesis conditions or $AlF_3 \cdot 3H_2O$ existence. These values are presented in Table S1. As the concentration of initial Ti_3AlC_2 is increased, there is a similar relationship to that seen by changing the etchant/MAX ratio, but it is not explicitly clear whether there is an upper region of concentration in which the $AlF_3 \cdot 3H_2O$ formation would decrease.
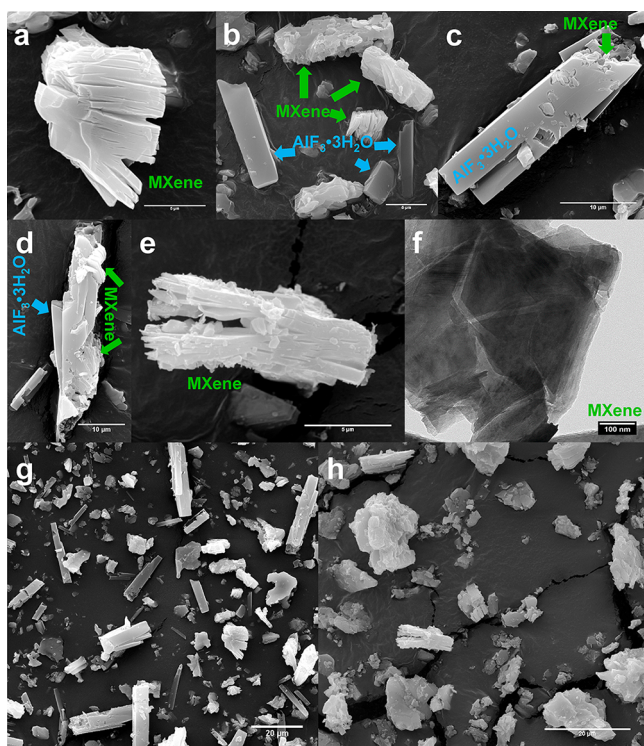
We used infrared (IR) spectroscopy to investigate surface bonding of representative samples. Near-room-temperature DRIFTS data are presented in Figure 4. The IR spectra of each sample show representative peaks of $Ti_3C_2T_x$ MXene and Ti_3AlC_2 MAX, especially characteristic peaks at ~1250, 1100, and 900 cm^{-1}.[12−14] The MAX parent phase IR spectra are shown in Figure S2. The high $AlF_3 \cdot 3H_2O$ sample (5.0-CoF_2/MAX) presents characteristic IR bands of $AlF_3 \cdot 3H_2O$.[15] Specifically, crystalline water (O−H bond) is identified from the peak at ~1700 cm^{-1} and from the broad shoulder from ~4000 to 3200 cm^{-1}, and Al−F bonding is distinguished from the heads emerging at ~800 and ~700 cm^{-1}. This spectroscopic evidence supports our structural analysis by providing the bonding evolution as the etching condition varies.

Morphological investigations into the high and low $AlF_3 \cdot 3H_2O$ content samples were conducted. The morphology of the cobalt fluoride etched MXenes was revealed by SEM. Shown in Figure 5a is a representative particle of $Ti_3C_2T_x$ pure phase MXene. Figure 5a presents a typical "open book" layered structure very similar to MXenes etched by other methods.

Figure 4. DRIFTS data of $Ti_3C_2T_x$ etched at a 4 wt % with different CoF_2/MAX molar ratios from 4000 to 2500 cm^{-1} and from 1850 to 600 cm^{-1} at 50 °C.

Figure 5b−d presents the morphology of being "$AlF_3 \cdot 3H_2O$ rich". Both homogeneous (single phase) $AlF_3 \cdot 3H_2O$ (Figure 5b) and heterogeneous MXene/$AlF_3 \cdot 3H_2O$ particles (Figure 5c,d) are clearly identified. $AlF_3 \cdot 3H_2O$ particles are cubic rods that present highly resolved sharp edges and smooth surfaces.[7] In contrast, the MXene particles, both free of $AlF_3 \cdot 3H_2O$ and with $AlF_3 \cdot 3H_2O$ embedded, appear to have much less uniform morphology with rough surfaces attributed to its layered stacking.[1,2] It is very likely that such heterogeneity originates from $AlF_3 \cdot 3H_2O$ crystallization within the interlayer space or on the internal surfaces of the MXene samples. Such a phenomenon may disrupt the formation of homogeneously stacked MXene layers by formation of a series of hybrid MXene/$AlF_3 \cdot 3H_2O$ structures, which is also evidenced by large distribution of interlayer spaces (wide (002) peaks) seen in the $AlF_3 \cdot 3H_2O$ rich samples. The SEM of the 5.0-CoF_3/MAX-4, showing no $AlF_3 \cdot 3H_2O$ and poor crystallinity in XRD (Figure 2b), does not show large $AlF_3 \cdot 3H_2O$ particles as seen in 5.0-CoF_2/MAX-4 but does show small particles dotting MXene as seen in Figure 5e. This "overetched" MXene is speckled with interlayer particles. These particles are anticipated to be $AlF_3 \cdot 3H_2O$ that are too small to be appreciably detected by XRD;

Figure 5. (a−d) 5.0-CoF$_2$/MAX-4, (e) 5.0-CoF$_3$/MAX-4, (f) TEM of 3.6-CoF$_2$/MAX-4, (g) 5.0-CoF$_2$/MAX-4 zoomed out view, and (h) 5.0-CoF$_3$/MAX-4 zoomed out view.

alternatively, the deposits could be TiO$_2$ particles oxidized from surface titanium groups, similar to FeF$_3$ etched MXenes oxidation in water to form a TiO$_2$ coated Ti$_3$C$_2$T$_x$ morphology.[7] Figure 5f presents a top-down view of the Ti$_3$C$_2$T$_x$'s morphology using TEM. The stacking of layers of MXene is along the edges of the particle as apparent striations, the darker sections of the particle being the more densely layered sections. This particle shows representative morphology of well etched MXenes.[2,16] By control of CoF$_2$/MAX, the morphology of MXene can be tuned to provide different MXene and AlF$_3$·3H$_2$O structures, including typical pristine "open book" particles that are common to MXenes (Figure 5a,f). Not investigated here, morphology could further be manipulated using delamination methods for a more exfoliated structure or single layers.[9,17] The morphology of MXene is directly affected by AlF$_3$·3H$_2$O content, being embedded in large AlF$_3$·3H$_2$O rods and also having AlF$_3$·3H$_2$O particles in interlayer spacings upon drying, but good morphology is shown from near-pure MXene samples etched by CoF$_2$ environment.

A direct comparison of the TG−DSC−MS curves of three samples, 3.6-, 5.0-, and 7.5-CoF$_2$/MAX-4, is shown in Figure 6, each sample representing below the region of AlF$_3$·3H$_2$O formation, inside, and above, respectively. Using TG-DSC-MS affords the parallel investigation of mass content, energetic evolutions, and guest−host (water−MXene) interactions. Considering 3.6-CoF$_2$/MAX-4 to be near-pure Ti$_3$C$_2$T$_x$ based on its XRD patterns and TEM, a baseline for MXene weight loss is constructed. By use of this baseline, the total mass loss of near-pure MXene is considered to be 6.8 wt % at 450 °C, which is high enough to expect near-total dehydration of AlF$_3$·3H$_2$O and below where Al$_2$O$_3$ and TiO$_2$ form.[15,18] Then, using the theoretical weight loss of dehydration of AlF$_3$·

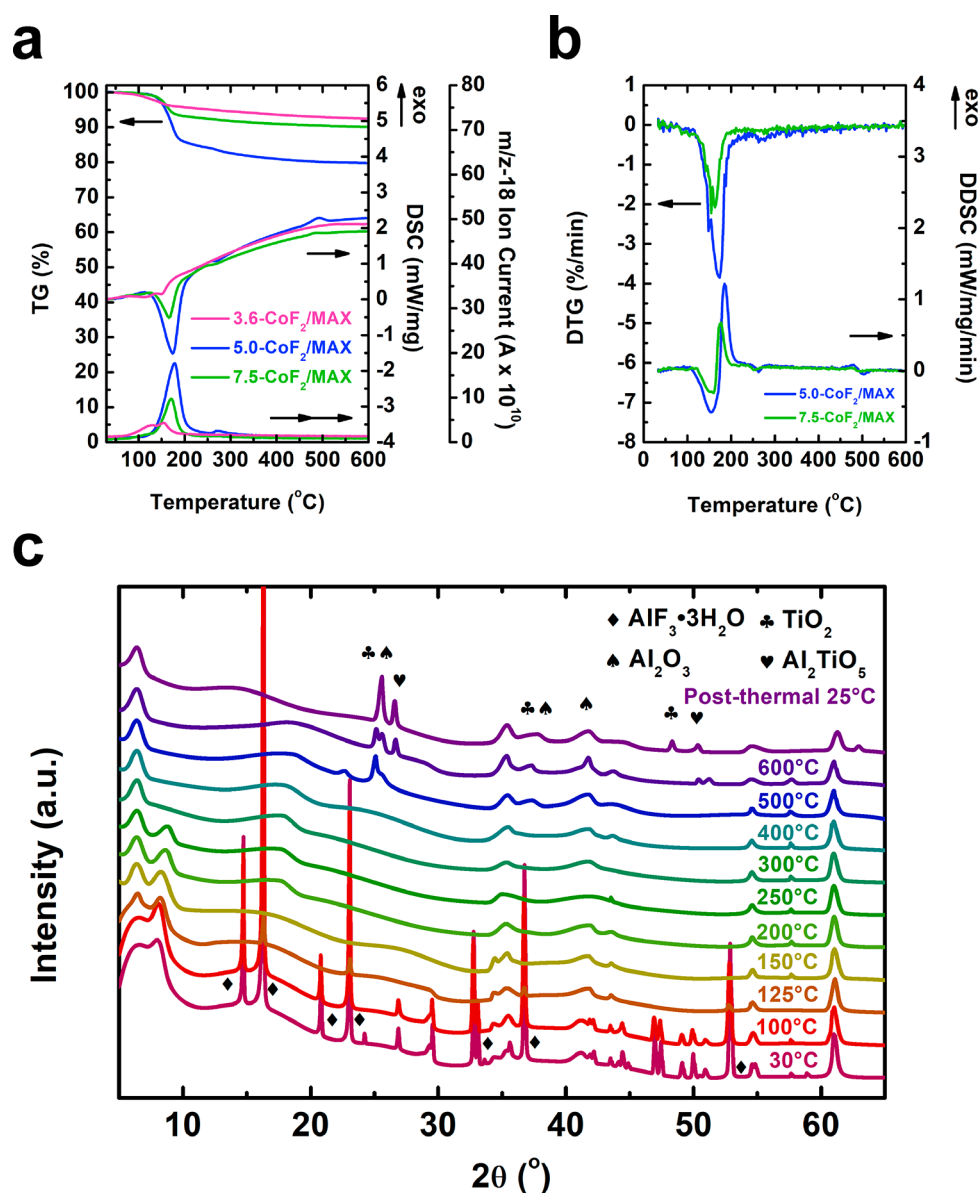3H$_2$O to be 38.9 wt %, we can estimate the content of CoF$_2$ etched samples by utilizing eq 2 below.

$$\text{wt \% of AlF}_3\cdot3\text{H}_2\text{O}$$
$$= \frac{\text{sample wt \% loss} - \text{wt \% loss of near-pure MXene}}{\text{theoretical wt \% loss of AlF}_3\cdot3\text{H}_2\text{O} - \text{wt \% loss of near-pure MXene}}$$
$$\times 100 \ (\%) \tag{2}$$

According to the thermal analysis, the AlF$_3$·3H$_2$O weight percentages are estimated to be 39.8 and 8.0 wt % in 5.0- and 7.5-CoF$_2$/MAX-4, respectively (see Table 1). This is in excellent agreement with the XRD data that there exists a region of AlF$_3$ speciation stability at moderate ratios of CoF$_2$.

By use of thermal analysis, near-pure Ti$_3$C$_2$T$_x$ (3.6-CoF$_2$/MAX-4) and high AlF$_3$·3H$_2$O content Ti$_3$C$_2$T$_x$ (5.0- and 7.5-CoF$_2$/MAX-4) was analyzed in-depth with emphasis on dehydration mechanisms. The two endothermic DSC peaks of 3.6-CoF$_2$/MAX-4 in Figure 6a suggest a double-stage dehydration. Specifically, in stage 1, the broad DSC peak spanning from 90 to 136 °C suggests the loss of loosely attached or intercalated water. In stage 2 a very well-resolved DSC signal is seen at ∼151 °C, which indicates a family of more tightly bound water under energetically similar confinement (intercalation) environments. According to earlier studies, the water desorbed in stage 2 interacts with surface groups such as −OH via hydrogen bonding.[19,20] The presence of two distinct types of water is also shown by the MS (m/z = 18) curves shown in Figure 6a. On the other hand, for samples containing appreciably amounts of AlF$_3$·3H$_2$O (5.0- and 7.5-CoF$_2$/MAX-4), the dehydration is primarily owing to decomposition of AlF$_3$·3H$_2$O.[18] Specifically, the first sharp endothermic peak occurring at ∼170 °C indicates the loss of the majority of the crystalline water of AlF$_3$·3H$_2$O. From 110 to 220 °C, AlF$_3$·3H$_2$O dehydrates to AlF$_3$·0.5H$_2$O. Subsequently, the second stage of dehydration takes place between 260 and 280 °C leading to full dehydration of AlF$_3$·0.5H$_2$O to α-AlF$_3$. This endothermic event, although not obvious in the DSC−MS curves, is clearly identified when taking the derivative of the TG (DTG) and DSC (DDSC) curves. The DTG and DDSC profiles of 5.0- and 7.5-CoF$_2$/MAX-4 (see Figure 6b) highlight the subtle weight losses and endothermic thermal events at about 260 °C. The DTG−DDSC curves suggest rapid weight loss and heat absorption between 150 and 200 °C, corresponding to the first step in AlF$_3$·3H$_2$O dehydration. At ∼260 °C, a small weight loss associated with an endothermic heat effect, corresponding to the second step of the dehydration of AlF$_3$·0.5H$_2$O, is identified. Interestingly, a minor exothermic event occurring at ∼490 °C implying the oxidation of surface titanium into TiO$_2$ and α-AlF$_3$ into Al$_2$O$_3$ by residual water is observed, as evidenced by the identification via *in situ* XRD of TiO$_2$ and Al$_2$O$_3$ present at 500 °C (see Figure 6c). The dehydration of AlF$_3$·3H$_2$O dominates the thermal analysis of Ti$_3$C$_2$T$_x$ with even low amounts of AlF$_3$·3H$_2$O. This qualitative thermal analysis further reinforces the conclusions drawn in the quantitative thermal, structural, and spectroscopic analyses.

Further *in situ* structural study is performed to assist the quantitative thermal analysis, using the ratio of representative peak intensities of AlF$_3$·3H$_2$O to Ti$_3$C$_2$T$_x$ to elucidate a clear trend. Observed is a link from the ionic strength of solution to the AlF$_3$·3H$_2$O formation content, Figure 7. High intensity/intensity ratios are observed between 8.5 and 10 M, while below and above, less than 1:1 is seen. With higher intensity

Figure 6. (a) TG−DSC−MS curves of $Ti_3C_2T_x$ etched at 4 wt % with different CoF_2/MAX molar ratios at a scan rate of 10 °C/min. (b) DTG−DDSC curves of $Ti_3C_2T_x$ etched at 4 wt % with 5.0 and 7.5 CoF_2/MAX molar ratios at a scan rate of 10 °C/min. (c) In situ XRD of 5.0-CoF_2/MAX-4 at a heating rate of 10 °C/min under a helium flow of 50 mL/min.

Table 1. $AlF_3·3H_2O$ Content and Corresponding Total Mass Loss at 450 °C from TG Curves with Samples of 4 wt % MAX Phase
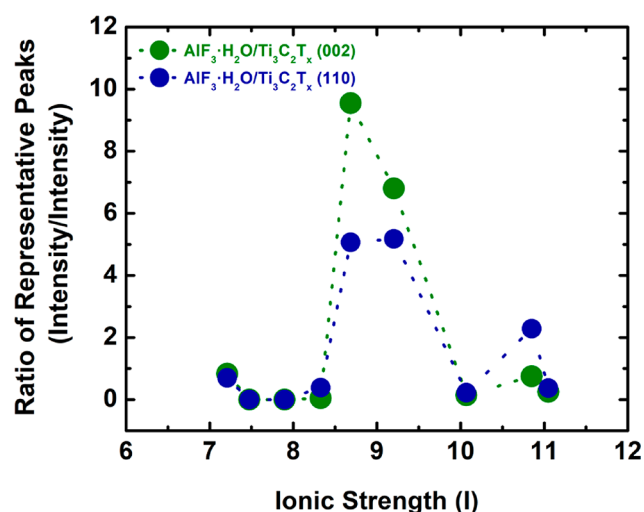
ratio of CoF_2/MAX	mass loss at 450 °C (wt %)	$AlF_3·3H_2O$ (wt %)[a]
3.6[b]	6.8	0
5	19.6	39.8
7.5	9.3	8.0

[a]Calculated from eq 1. [b]Sample 3.6-CoF_2/MAX-4 is assumed to be near-pure MXene from its structural and spectroscopic analysis.

ratios there is found a greater disparity between the ratios found using (002) and (110) peaks. This is due to the greater widths of the (002) peaks with respect to the (110) peaks (indicative of the *a* lattice parameter), meaning that there is a larger distribution in the *c* lattice parameters and therefore the interlayer spacings in the high $AlF_3·3H_2O$ content samples. $AlF_3·3H_2O$ directly affects the distribution of interlayer

spacings of $Ti_3C_2T_x$, supposedly due to inconsistent $AlF_3·3H_2O$ growth outside and between $Ti_3C_2T_x$ layers. A normal distribution is expected from the complexation of AlF_3 in solution in a region of certain ionic strength and pH.[10] On the basis of known complexation of AlF_3, a clear trend is observed in Figure 7 implying a region of AlF_3 complex stability. Here, at a pH of −0.78, due to the high concentration of HCl (6 M), AlF_3 complexation is highly stable between 8.5 and 10 M as evidenced by the high ratio of representative peak intensities of $AlF_3·3H_2O$ to $Ti_3C_2T_x$. At greater or less ionic strengths, AlF^{2+}, AlF_2^+, AlF_4^-, AlF_5^{2-}, and AlF_6^{3-} complexes which remain aqueous will be majority thermodynamically preferred. These are simply washed out postsynthesis. The relative lattice parameter comparison shows that high and low $AlF_3·3H_2O$ wt. % samples correspond to ionic strengths, those being within 8.5 and 10 M showing high $AlF_3·3H_2O$ content, and the $AlF_3·3H_2O$ wt % estimated from the thermal analysis directly supports this trend.

Figure 7. Ratio of AlF$_3$·3H$_2$O's representative peak intensity (observed at 17°) to the Ti$_3$C$_2$T$_x$'s peak intensity of (002) (corresponding to the c lattice parameter), green dots, and (110) (corresponding to the a lattice parameter), navy dots, by ionic strength of solution (I) during synthesis from XRD patterns retrieved from Figures 2, 3, and 4.

In the MXene etching environment, formation of AlF$_3$·3H$_2$O depends strongly on the ionic strength of solution. The ionic strength of solution directly effects Al−F complexation. AlF$_3$·3H$_2$O formation is expected when AlF$_3$ complexation is thermodynamically stable. A region of thermodynamic stability of AlF$_3$ complexation is seen from the trend between ionic strength of solution during synthesis and the AlF$_3$·3H$_2$O peak ratios to Ti$_3$C$_2$T$_x$. Because AlF$_3$ will crystallize with H$_2$O, there is also a kinetic factor to acknowledge when considering synthesis, not explored here, but seen by the qualitative increase in AlF$_3$·3H$_2$O content by increasing etching times when etched with HF.[8] Ti$_3$C$_2$T$_x$'s surfaces may be favorable for AlF$_3$·3H$_2$O precipitation as evidenced by hybrid Ti$_3$C$_2$T$_x$/AlF$_3$·3H$_2$O particles which appear to have AlF$_3$·3H$_2$O around and inside Ti$_3$C$_2$T$_x$, some with particles seen even between layers (Figure 5c−e). The interlayer AlF$_3$·3H$_2$O particles seen in the interlayer space of MXene could form in the interlayer space or, alternatively, could be formed in solution and then agglomerate within the available interlayer spaces of MXenes during drying. For near-pure MXene, synthesis design should consider the pH and ionic strength of solution to avoid the region of AlF$_3$ complexation, or conversely, by purposely synthesizing MXene in a stable AlF$_3$ complexation region, syntheses could reliably incorporate AlF$_3$·3H$_2$O.

Electrochemical investigations into cobalt fluoride etched MXenes and their MXene/AlF$_3$·3H$_2$O hybrid structure are being performed by our group to evaluate their performance as electrode materials. An integrated calorimetric and structural investigation into the MXenes's behavior under thermal treatment will soon be presented on cobalt fluoride etched MXenes, emphasizing structural and surface bonding evolutions.

CONCLUSIONS

CoF$_2$ and CoF$_3$ were used to form HF *in situ* with HCl for a unique etching environment used to synthesize Ti$_3$C$_2$T$_x$ MXene from Ti$_3$AlC$_2$ MAX followed by structural, morphologic, spectroscopic, and thermal analyses. The most critical

conclusion is that the formation of AlF$_3$·3H$_2$O was demonstrated to be dependent on the ionic strength of solution through its direct effect on the thermodynamic stability of the AlF$_3$ complex. Specifically, when AlF$_3$ complexation is stable, between approximately I (ionic strength) = 8.5 M and 10 M, AlF$_3$·3H$_2$O/Ti$_3$C$_2$T$_x$ hybrid structures are evidenced. In sharp contrast, there is no AlF$_3$·3H$_2$O precipitate when I is smaller than 8.5 or larger than 10 M. In other words, near-pure MXene phase is the only solid product. Therefore, by manipulating the ionic strength, I, of the etching environment, the formation of AlF$_3$·3H$_2$O can be accurately controlled to achieve MXenes with high purity or to intentionally create Ti$_3$C$_2$T$_x$/AlF$_3$·3H$_2$O hybrids.

◼ ASSOCIATED CONTENT

ⓢ Supporting Information

The Supporting Information is available free of charge on the ACS Publications website at DOI: 10.1021/acsaem.9b01618.

> Low etchant/MAX ratio XRD patterns; DRIFTS of MAX; lattice parameter and unit cell volumes of Ti$_3$C$_2$T$_x$ samples (PDF)

◼ AUTHOR INFORMATION

Corresponding Author

*E-mail: d.wu@wsu.edu.

ORCID ⓘ

Junming Sun: 0000-0002-0071-9635
Steven R. Saunders: 0000-0001-6714-7435
Yong Wang: 0000-0002-8460-7410
Di Wu: 0000-0001-6879-321X

Notes

The authors declare no competing financial interest.

◼ REFERENCES

(1) Naguib, M.; Kurtoglu, M.; Presser, V.; Lu, J.; Niu, J.; Heon, M.; Hultman, L.; Gogotsi, Y.; Barsoum, M. W. Two-Dimensional Nanocrystals Produced by Exfoliation of Ti$_3$AlC$_2$. *Adv. Mater.* **2011**, 23 (37), 4248−4253.

(2) Anasori, B.; Lukatskaya, M. R.; Gogotsi, Y. 2D Metal Carbides and Nitrides (MXenes) for Energy Storage. *Nat. Rev. Mater.* **2017**, 2, 16098.

(3) Xiong, D.; Li, X.; Bai, Z.; Lu, S. Recent Advances in Layered Ti$_3$C$_2$T$_x$ MXene for Electrochemical Energy Storage. *Small* **2018**, 14 (17), 1703419.

(4) Zhu, J.; Ha, E.; Zhao, G.; Zhou, Y.; Huang, D.; Yue, G.; Hu, L.; Sun, N.; Wang, Y.; Lee, L. Y. S.; Xu, C.; Wong, K. Y.; Astruc, D.; Zhao, P. Recent Advance in MXenes: A Promising 2D Material for Catalysis, Sensor and Chemical Adsorption. *Coord. Chem. Rev.* **2017**, 352, 306−327.

(5) Verger, L.; Natu, V.; Carey, M.; Barsoum, M. W. MXenes: An Introduction of Their Synthesis, Select Properties, and Applications. *Trends Chem.* **2019**, *1*, 656−669.

(6) Ronchi, R. M.; Arantes, J. T.; Santos, S. F. Synthesis, Structure, Properties and Applications of MXenes: Current Status and Perspectives. *Ceram. Int.* **2019**, *45* (15), 18167−18188.

(7) Wang, X.; Garnero, C.; Rochard, G.; Magne, D.; Morisset, S.; Hurand, S.; Chartier, P.; Rousseau, J.; Cabioc'H, T.; Coutanceau, C.; Mauchamp, V.; Celerier, S. A New Etching Environment (FeF$_3$/HCl) for the Synthesis of Two-Dimensional Titanium Carbide MXenes: A Route towards Selective Reactivity: Vs. Water. *J. Mater. Chem. A* **2017**, *5* (41), 22012−22023.

(8) Rajavel, K.; Ke, T.; Yang, K.; Lin, D. Condition Optimization for Exfoliation of Two Dimensional Titanium Carbide (Ti$_3$C$_2$T$_X$). *Nanotechnology* **2018**, *29* (9), 095605.

(9) Alhabeb, M.; Maleski, K.; Anasori, B.; Lelyukh, P.; Clark, L.; Sin, S.; Gogotsi, Y. Guidelines for Synthesis and Processing of Two-Dimensional Titanium Carbide (Ti$_3$C$_2$T$_x$ MXene). *Chem. Mater.* **2017**, *29* (18), 7633−7644.

(10) Corbillon, M. S.; Olazabal, M. A.; Madariaga, J. M. Potentiometric Study of Aluminium-Fluoride Complexation Equilibria and Definition of the Thermodynamic Model. *J. Solution Chem.* **2008**, *37* (4), 567−579.

(11) Gong, W. X.; Qu, J. H.; Liu, R. P.; Lan, H. C. Effect of Aluminum Fluoride Complexation on Fluoride Removal by Coagulation. *Colloids Surf., A* **2012**, *395*, 88−93.

(12) Yan, P.; Zhang, R.; Jia, J.; Wu, C.; Zhou, A.; Xu, J.; Zhang, X. Enhanced Supercapacitive Performance of Delaminated Two-Dimensional Titanium Carbide/Carbon Nanotube Composites in Alkaline Electrolyte. *J. Power Sources* **2015**, *284*, 38−43.

(13) Han, Y.-H.; Deng, Q.; Huang, Q.; Du, S.; Zhou, X.; Li, Y.; Lee, J.; Wang, J.; Li, M. Facile Preparation of in Situ Coated Ti$_3$C$_2$T$_x$/Ni$_{0.5}$Zn$_{0.5}$Fe$_2$O$_4$ Composites and Their Electromagnetic Performance. *RSC Adv.* **2017**, *7* (40), 24698−24708.

(14) Zhi, W.; Xiang, S.; Bian, R.; Lin, R.; Wu, K.; Wang, T.; Cai, D. Study of MXene-Filled Polyurethane Nanocomposites Prepared via an Emulsion Method. *Compos. Sci. Technol.* **2018**, *168*, 404−411.

(15) Alonso, C.; Morato, A.; Medina, F.; Guirado, F.; Cesteros, Y.; Salagre, P.; Sueiras, J. E.; Terrado, R.; Giralt, A. Preparation and Characterization of Different Phases of Aluminum Trifluoride. *Chem. Mater.* **2000**, *12* (4), 1148−1155.

(16) Ghidiu, M.; Lukatskaya, M. R.; Zhao, M. Q.; Gogotsi, Y.; Barsoum, M. W. Conductive Two-Dimensional Titanium Carbide "clay" with High Volumetric Capacitance. *Nature* **2014**, *516* (7529), 78−81.

(17) Naguib, M.; Unocic, R. R.; Armstrong, B. L.; Nanda, J. Large-Scale Delamination of Multi-Layers Transition Metal Carbides and Carbonitrides "MXenes". *Dalt. Trans.* **2015**, *44* (20), 9353−9358.

(18) Delong, X.; Yongqin, L.; Ying, J.; Longbao, Z.; Wenkui, G. Thermal Behavior of Aluminum Fluoride Trihydrate. *Thermochim. Acta* **2000**, *352−353*, 47−52.

(19) Seredych, M.; Shuck, C. E.; Pinto, D.; Alhabeb, M.; Precetti, E.; Deysher, G.; Anasori, B.; Kurra, N.; Gogotsi, Y. High-Temperature Behavior and Surface Chemistry of Carbide MXenes Studied by Thermal Analysis. *Chem. Mater.* **2019**, *31* (9), 3324−3332.

(20) Thakur, R.; VahidMohammadi, A.; Moncada, J.; Adams, W. R.; Chi, M.; Tatarchuk, B.; Beidaghi, M.; Carrero, C. A. Insights into the Thermal and Chemical Stability of Multilayered V$_2$CT$_x$ MXene. *Nanoscale* **2019**, *11*, 10716−10726.